

Nodal superconductivity coexists with low-moment static magnetism in single-crystalline tetragonal FeS: A muon spin relaxation and rotation study

C. Tan,¹ T. P. Ying,¹ Z. F. Ding,¹ J. Zhang,¹ D. E. MacLaughlin,² O. O. Bernal,³ P. C. Ho,⁴ K. Huang,^{1,5} I. Watanabe,⁶ S. Y. Li,^{1,7} and L. Shu^{1,7,*}

¹State Key Laboratory of Surface Physics, Department of Physics, Fudan University, Shanghai 200433, China

²Department of Physics and Astronomy, University of California, Riverside, California 92521, USA

³Department of Physics and Astronomy, California State University, Los Angeles, California 90032, USA

⁴Department of Physics, California State University, Fresno, California 93740, USA

⁵National High Magnetic Field Laboratory, Tallahassee, Florida 32310, USA

⁶Advanced Meson Science Laboratory, RIKEN Nishina Center, Wako 351-0198, Japan

⁷Collaborative Innovation Center of Advanced Microstructures, Nanjing 210093, China



(Received 29 January 2018; revised manuscript received 15 May 2018; published 31 May 2018)

We report muon spin relaxation and rotation (μ SR) measurements on hydrothermally grown single crystals of superconducting tetragonal FeS, which help to clarify the controversial magnetic state and superconducting gap symmetry of this compound. μ SR time spectra were obtained from 280 K down to 0.025 K in zero field (ZF) and applied fields up to 75 mT. In ZF, the observed loss of initial asymmetry (signal amplitude) and increase of depolarization rate Λ_{ZF} below 13 K indicate the onset of static magnetism, which coexists with superconductivity below T_c . TF μ SR results indicate a linear temperature dependence of the superfluid density at low temperature, consistent with nodal superconductivity. The $s+d$ -wave model gives the best fit to the observed temperature and field dependencies, and yields an in-plane penetration depth value $\lambda_{ab}(T=0) = 241(3)$ nm.

DOI: [10.1103/PhysRevB.97.174524](https://doi.org/10.1103/PhysRevB.97.174524)

I. INTRODUCTION

The discovery of superconducting $\text{La}(\text{O}_{1-x}\text{F}_x)\text{FeAs}$ [1] has triggered extensive studies on iron-based superconductors (IBS) [2,3]. Most of the IBS share the same common structural motif of Fe-As layers, and the highest T_c value is up to 56 K [4,5]. Density-functional theory (DFT) calculations showed similarities of Fermi-surface structure between Fe-As-based superconductors and iron chalcogenides (FeSe, FeS, and FeTe) [6]. These compounds have the simplest crystal structure (iron chalcogenide layers) of the IBS, and have therefore attracted great interest [7]. FeSe, the most studied iron chalcogenide, becomes superconducting below $T_c = 8$ K [8], which is a lower transition temperature than many iron arsenide superconductors. However, T_c increases drastically under pressure [9] by carrier doping [10] or by growing single-layer FeSe on a SrTiO_3 substrate [11,12]. Nematic order [13] occurs in bulk FeSe below $T_s = 90$ K [14], and antiferromagnetic (AFM) order is absent [15,16]. This makes FeSe a clean platform to study the nature of Fe-based superconductivity. However, its superconducting gap structure remains controversial [17–19].

Recently, superconducting tetragonal FeS ($T_c \approx 4.5$ K) was successfully synthesized by Lai *et al.* [20] using a hydrothermal method. It has the same structure as FeSe, with selenium replaced by sulfur. Many studies have been made to understand the magnetic state and superconducting gap symmetry of FeS. Notably, two superconducting domes were observed under

pressure [21], posing challenges to understanding its pairing mechanism.

The muon spin relaxation/rotation (μ SR) technique [22–24] has been used to study superconductivity in polycrystalline tetragonal FeS [25,26]. These experiments indicated fully gapped superconductivity, and found low-moment disordered magnetism below $T_{\text{mag}} \approx 20$ K [25]. However, a nodal superconducting gap was observed in single-crystalline FeS by low temperature specific heat and thermal conductivity measurements [27,28]. Yang *et al.* [29] calculated the electronic structure of FeS using DFT and reported that the gap function is nodal/nodeless on the hole/electron Fermi pockets. Soon after, angle-resolved photoemission spectroscopy (ARPES) studies [30] observed two holelike and two electronlike Fermi pockets around the Brillouin zone center and corner, respectively. The authors attribute the controversies over the superconducting gap structure to the absence of a holelike γ band, which had been observed in other IBS. As for the magnetic properties, Man *et al.* [31] concluded that FeS is a tetragonal paramagnet from elastic neutron scattering and transport measurements. This is consistent with a prediction of dynamical mean-field theory [32], but it contradicts the previous μ SR results [25].

To help resolve these controversies, we have performed μ SR experiments on single crystals of tetragonal FeS. Our ZF and longitudinal-field (LF) μ SR data reveal low-moment disordered static magnetism below $T_{\text{mag}} \approx 13$ K. Transverse field (TF) μ SR experiments in the superconducting state yield an in-plane superconducting penetration depth $\lambda_{ab}(0) = 241(3)$ nm. The data reveal a linear temperature dependence of λ_{ab}^{-2} as $T \rightarrow 0$, characteristic of an order parameter with line nodes (the quantity λ^{-2} is proportional to the superfluid density; in the

*leishu@fudan.edu.cn

following we use the two terms interchangeably). We conclude that the temperature dependencies of λ_{ab} measured at various applied fields are best described by a $s+d$ -wave model.

II. EXPERIMENTS AND RESULTS

Single-crystalline tetragonal FeS was prepared by deintercalation of potassium cations from $K_xFe_{2-y}S_2$ ($x \approx 0.8$, $y \approx 0.4$) single crystals by hydrothermal reaction [33,34]. Elemental analysis, x-ray diffraction (XRD), scanning electron microscopy image, magnetic susceptibility, and in-plane resistivity measurements were carried out, with results that are consistent with previously reported work [21,28]. Two batches of single crystal mosaics were prepared, denoted as Sample A and Sample B. μ SR experiments were performed at the M15 and M20 beam lines at TRIUMF, Vancouver, Canada [35]. ZF- and LF- μ SR measurements were carried out over the temperature range 25 mK–280 K for fields up to 20 mT. TF- μ SR measurements were performed from 6 K down to 25 mK in TFs $\mu_0 H_T = 7.5$ mT, 30 mT, and 75 mT. In all experiments, the positron detectors were aligned along the direction of the initial muon polarization. The evolution in time of the decay positron count asymmetry $A(t)$, which is proportional to the muon polarization, is often called a μ SR time spectrum.

A. ZF- and LF- μ SR

1. Constant terms in μ SR spectra

μ SR time spectra were measured with the fragile samples mounted on a silver backing plate [36]. The spectra contain a “background” contribution from muons that miss the sample and stop in the backing plate. In ZF or LF experiments, the total (sample + background) spectrum is given by

$$A(t)/A(0) = (1 - f_{Ag})G(t) + f_{Ag}, \quad (1)$$

where $A(0)$ is the initial magnitude of the total asymmetry, $G(t)$ is the sample relaxation function [$G(0) = 1$], and f_{Ag} is the fraction of muons that stop in the backing plate. For static muon relaxation (precession in a static distribution of local fields), in ZF or LF, $G(t)$ has the form [37,38]

$$G(t) = G'(t) + \text{const} \quad (2)$$

in the absence of dynamic relaxation. Here $G'(t)$ is due to the ensemble muon spin precession and decays to zero as the precession dephases the spins. The constant term in Eq. (2) is intrinsic to the sample, and is due to the components of the initial muon spins along the resultant of local and any applied LFs; these components do not precess and hence do not contribute to the relaxation. In ZF, the constant $f_{ZF} = 1/3$ for randomly oriented local fields [37,38]. It is greater or smaller than this value, respectively, if the local-field distribution is preferentially oriented parallel or perpendicular to the initial muon polarization.

The quantities f_{Ag} and f_{ZF} cannot be determined separately from ZF experiments alone, since they both contribute to the constant signal at late times. In TF- μ SR, however, there is no analog to f_{ZF} , and f_{Ag} is the fractional amplitude of the late-time oscillatory signal. It can be measured accurately if the sample signal decays rapidly, as is the case in our TF- μ SR

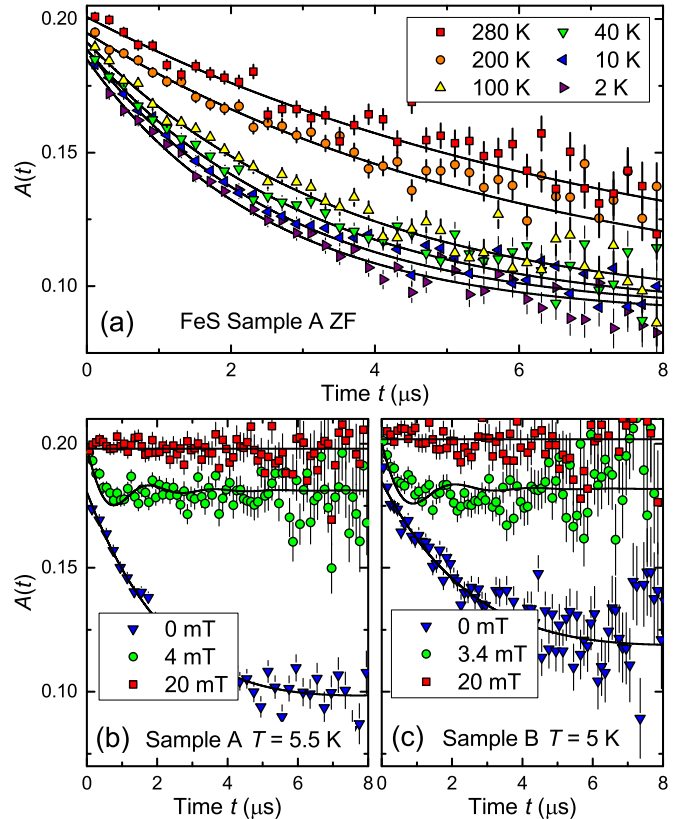


FIG. 1. μ SR time spectra from single-crystalline tetragonal FeS. (a) ZF- μ SR spectra at representative temperatures. Curves: Fits to the data by a simple exponential decay function [Eq. (3)]. (b)–(c) ZF- and LF- μ SR time spectra from samples A and B for various LFs H_L at 5 K. Curves: Fits of the LF Lorentzian Kubo-Toyabe function [24,39] to the LF data. The background signal from muons that stop in the silver backing plate has not been subtracted.

experiments at low temperatures (Sec. II B 1), where we obtain $f_{Ag} = 0.50(1)$ in a field of 30 mT. In ZF, f_{Ag} is essentially the same as in fields of this magnitude, since it depends only on the overlap of the muon beam with the backing plate. For the same reason, the background asymmetry $A_{Ag} \equiv A(0)f_{Ag}$ ($= 0.093(2)$ in ZF) is not expected to depend significantly on temperature.

2. Experimental results

In our ZF- and LF- μ SR experiments, the initial ensemble muon polarization \mathbf{P}_μ and applied LF \mathbf{H}_L (if present) were both parallel to the crystal c axis. Representative ZF- μ SR spectra between 2 K and 280 K are shown in Fig. 1(a).

The spectra are well described by a simple exponential decay function

$$A(t)/A(0) = (1 - f) \exp(-\Lambda_{ZF}t) + f, \quad (3)$$

at all temperatures, where Λ_{ZF} is the ZF muon depolarization rate and $f = 0.59(2)$ at low temperatures.

From Eqs. (1)–(3),

$$f_{ZF} = (f - f_{Ag})/(1 - f_{Ag}) = 0.18(6), \quad (4)$$

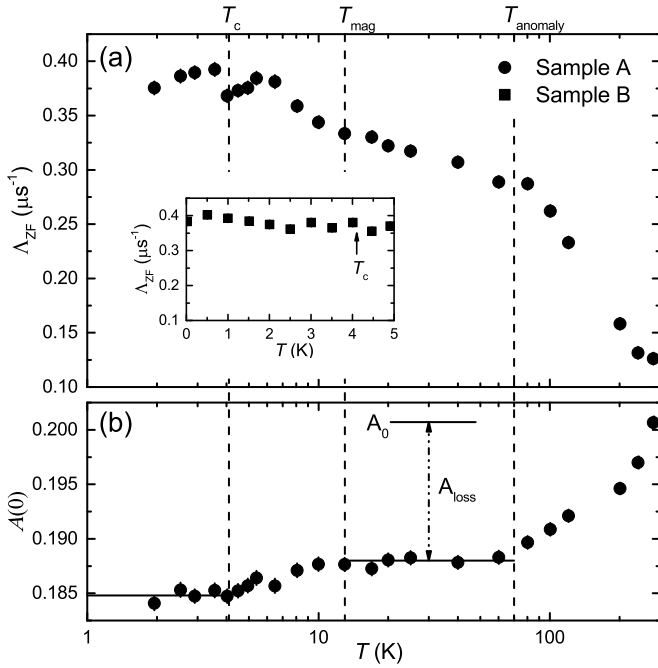


FIG. 2. (a) ZF muon depolarization rate Λ_{ZF} (square) versus logarithmic temperature for Sample B. Inset: the Λ_{ZF} (circle) versus temperature for Sample A. (b) Temperature dependence of initial asymmetry $A(0)$ for Sample B. Solid lines are guides to the eye. Loss of initial symmetry with decreasing temperature above ~ 70 K is attributed to a magnetic impurity phase (see text). The onset of static magnetism is evidenced by the additional increase of Λ_{ZF} and decrease of $A(0)$ below $T_{\text{mag}} \approx 13$ K.

indicating that local fields at muon sites are preferentially oriented in the ab plane. For Gaussian distributions of the local field with uniaxial symmetry [40], this value of f_{ZF} yields a rms width of the field distribution $\parallel \mathbf{c}$ roughly half that $\perp \mathbf{c}$. The observed depolarization is, however, clearly exponential and not Gaussian (cf. Fig. 1), thus this result is not a quantitative measure of the anisotropy. We note that the natural abundances and nuclear magnetic moments of both ^{57}Fe and ^{33}S are small [24], and the Gaussian Kubo-Toyabe (KT) relaxation expected from their dipolar fields is negligible.

Exponential muon depolarization is usually caused either by motionally narrowed dynamic relaxation, or by a Lorentzian static field distribution [24,39]. A longitudinal applied magnetic field $\mu_0 H_L \gg \Lambda_{ZF}/\gamma_\mu \approx 0.5$ mT, where $\gamma_\mu = 851.616$ MHz/T is the muon gyromagnetic ratio, “decouples” the local field [24,38,39] (i.e., prevents muon precession). As shown in Figs. 1(b) and 1(c), at 5 K, muon depolarization is completely suppressed in a field $\mu_0 H_L = 20$ mT, indicating that the local field is (quasi)static. The μSR spectra for intermediate fields can be fitted by the LF KT function appropriate to a randomly oriented Lorentzian static field distribution [39], although, as noted above, the local fields are preferentially oriented.

The temperature dependencies of Λ_{ZF} and the total observed initial asymmetry $A(0)$ [sample + background, Eq. (3)] are given in Fig. 2. The decrease of $A(0)$ with decreasing temperature above ~ 70 K is due to the onset of a strong local field in a fraction of the sample volume, so that muons in this volume

are rapidly depolarized and do not contribute to the signal [41]. This “lost” volume fraction $A_{\text{loss}}/(A_0 - A_{\text{Ag}})$, where $A_0 = 0.201(2)$ is the initial asymmetry at 300 K, increases with decreasing temperature to $\sim 12\%$ at 70 K. Magnetic susceptibility and XRD measurements on our FeS single crystals show no signature of spurious impurity phases, indicating that the volume fraction of second phase is much less than 12%. A similar loss of $A(0)$ was observed in ZF- μSR measurements on polycrystalline FeS samples [25], where it was attributed to small grains of a ferromagnetic impurity phase. These produce stray fields that affect an increasing fraction of the sample with decreasing temperature. Observation of these fields in both single-crystal and polycrystal FeS samples suggests that a spurious ferromagnetic phase is a byproduct of hydrothermally grown FeS [25,26].

The anomaly in $\Lambda_{ZF}(T)$ at 70 K (which was not reported in Ref. [25]) is close to a structural transition temperature for FeSe [14], and is reminiscent of the possibility of nematic order [13]. However, neither a structural transition nor nematic order has been observed in FeS [31,42]. The lattice parameters of tetragonal FeS decrease with decreasing temperature above 100 K, and remain almost constant below 100 K with a change of less than 1% from the value at 300 K [42]. Excluding these possibilities, the increase of $\Lambda_{ZF}(T)$ with decreasing temperature above 70 K is most probably due to increased local fields as discussed above. This in turn suggests a distribution of impurity-phase Curie temperatures T_C .

Between 13 K and 70 K, $A(0)$ is temperature independent. This is consistent with the anomaly in Λ_{ZF} at 70 K, and suggests that 70 K is the minimum in the distribution of impurity-phase T_C ; all grains are ferromagnetic below this temperature. The increase of Λ_{ZF} with decreasing temperature below 70 K is then probably intrinsic to FeS and dynamic, due to slowing down of intrinsic magnetic moment fluctuations. Future LF- μSR experiments will be necessary to determine separate static and dynamic contributions to Λ_{ZF} in this temperature range.

From 13 K to $\sim T_C$, $A(0)$ decreases slightly [$A(0)$], and $\Lambda_{ZF}(T)$ increases further, indicating a second source of static magnetism with a distribution of ordering temperatures [41]. The absence of oscillations in ZF- μSR spectra [Fig. 1(a)] indicates that this static magnetism is also disordered. The exponential form of the muon depolarization discussed in Sect. II A 2 is expected in dilute spin glasses [39], where the required Lorentzian field distribution is a consequence of the $1/r^3$ spatial dependence of the dipolar local field, but a “Lorentzian” distribution can arise from aspects of the disorder other than dilution. Here the origin is probably low-moment short-range static magnetism [25] with considerable inhomogeneity.

If we assume that the muon site in FeS is the same as calculated for isostructural FeSe [43], then $\Lambda_{ZF} \sim 0.4 \mu\text{s}^{-1}$ corresponds to an Fe magnetic moment of the order of $10^{-3} \mu_B$ [25]. Such a small moment would be undetectable by neutron diffraction. It should be noted, however, that the calculated muon stopping site [43] possesses a high point symmetry, so that partial cancellation of local fields is possible if the short-range correlation is AFM. The above estimate does not take this into account, so that the actual Fe magnetic moment could be considerably higher.

Below, T_c Λ_{ZF} saturates at $\sim 0.4\mu\text{s}^{-1}$, and $A(0)$ is again constant. Here exponential relaxation characterizes the entire observed sample signal, i.e., $\sim 85\%$ of the sample volume [Fig. 2(b)]. In ZF, no signature of the superconducting transition is expected. However, superconducting-state relaxation also characterizes the entire TF- μSR sample signal (Sec. II B 1). This is evidence that low-moment static magnetism coexists microscopically with superconductivity without the competition observed in other IBS [44–46].

B. TF- μSR

In a type-II superconductor, an applied magnetic field can induce a flux line lattice (FLL), in which the distribution of the field is determined by the magnetic penetration depth λ , the vortex core radius ξ , and the structure of the FLL [47]. The distribution of precession frequencies in a FLL and resulting loss of ensemble muon spin polarization reflect the field inhomogeneity, and quantities such as penetration depth λ can be extracted from the μSR spectra [24,48].

For a perfect FLL, the distribution of internal field is highly asymmetric, far from either a Gaussian or a Lorentzian field distribution. Weak random pinning slightly distorts the FLL so that the extrema of the field distribution fluctuate spatially; this often makes a Gaussian field distribution a good approximation [47]. The muon spin depolarization rate $\sigma_{\text{sc}} = \gamma_{\mu} \Delta B_{\text{rms}}$, where ΔB_{rms} is the rms width of the internal field distribution in the FLL. In turn, ΔB_{rms} is approximately related to the penetration depth λ_{ab} by [25,49]

$$\Delta B_{\text{rms}} = 0.172 \frac{\Phi_0}{2\pi} (1-b)[1 + 1.21(1 - \sqrt{b})^3] \lambda_{ab}^{-2}, \quad (5)$$

where $\Phi_0 = 2.068 \times 10^{-15}$ Wb is the magnetic flux quantum and $b = B/B_{c2} \approx H_T/H_{c2}(T)$. Equation (5) is a good approximation for $\kappa = \lambda/\xi \gtrsim 5$ and $1 > b \gtrsim 0.25/\kappa^{1.3}$ [49], which is appropriate to FeS below T_c and $H_T \geq 30$ mT.

1. Experimental results

In our TF- μSR experiments, the orientations of the initial muon spin polarization \mathbf{P}_{μ} and the applied field \mathbf{H}_T relative to the crystal c axis were $\mathbf{P}_{\mu} \perp \mathbf{c}$ and $\mathbf{H}_T \parallel \mathbf{c}$, respectively. TF- μSR data were taken after cooling from the normal state in constant field, to avoid spurious field inhomogeneity due to flux trapping if the field is changed below T_c . Figure 3(a) gives representative TF- μSR spectra for FeS Sample B at $\mu_0 H_T = 30$ mT above and below T_c . These spectra are well described by the TF muon depolarization function

$$A(t) = (A(0) - A_{\text{Ag}}) \exp\left(-\Lambda_{\text{TF}} t - \frac{1}{2} \sigma_{\text{sc}}^2 t^2\right) \cos(\gamma_{\mu} B t + \varphi) + A_{\text{Ag}} \cos(\gamma_{\mu} B_{\text{ext}} t + \varphi_{\text{Ag}}), \quad (6)$$

where Λ_{TF} is the depolarization rate due to static magnetism (in analogy to Λ_{ZF}), σ_{sc} is the Gaussian depolarization rate due to the FLL, B and φ are the mean field and initial phase of the ensemble muon precession, respectively, and A_{Ag} is the background signal asymmetry discussed in Sec. II A 1. The muon depolarization above T_c is due only to static magnetism, and exhibits a simple exponential character similar to ZF data

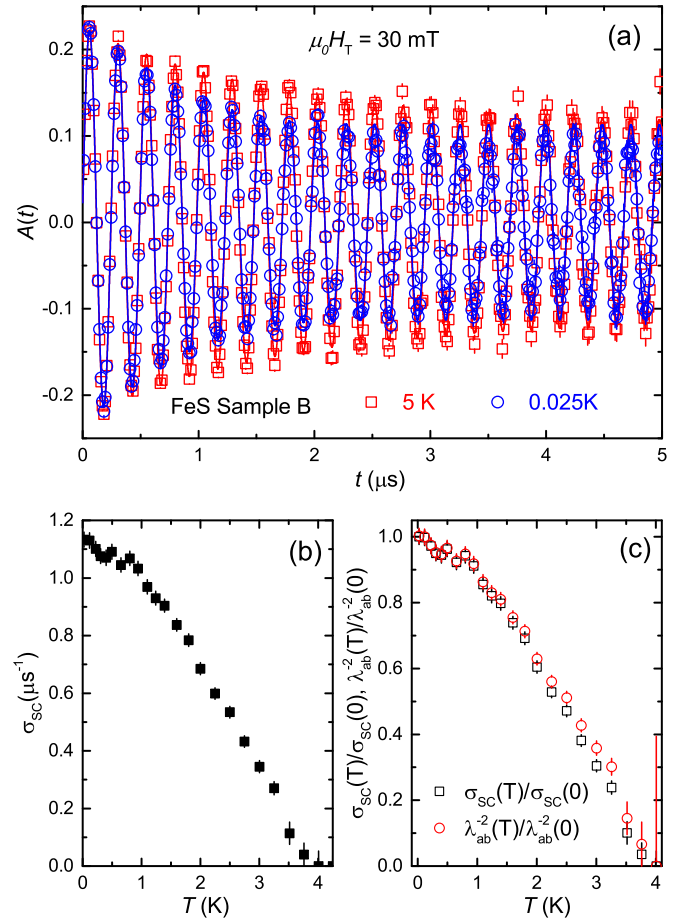


FIG. 3. TF- μSR data from FeS Sample B, $\mu_0 H_T = 30$ mT. (a) Time spectra for FeS Sample B above (squares) and below (circles) the superconducting transition temperature $T_c = 4.1$ K. Curves: Fits of Eq. (6) to the data. The additional muon depolarization below T_c is due to the field distribution in the FLL. (b) Temperature dependence of the Gaussian depolarization rate σ_{sc} from fits of Eq. (6) to TF- μSR data measured at $\mu_0 H = 30$ mT. (c) Temperature dependence of $\sigma_{\text{sc}}(T)/\sigma_{\text{sc}}(0)$ (squares) and $\lambda_{ab}^{-2}(T)/\lambda_{ab}^{-2}(0)$ (circles). See main text for details.

(Fig. 1). Above T_c , $\Lambda_{\text{TF}} \approx 0.63\mu\text{s}^{-1}$, which is slightly larger than Λ_{ZF} . This suggests that the applied field orients the local field slightly along the c axis.

Below T_c , the additional muon depolarization due to the FLL is well fit by the Gaussian term in Eq. (6) with Λ_{TF} fixed to its value above T_c . This is consistent with association of both exponential and Gaussian relaxation with the observed sample-component signal (initial asymmetry $A(0) - A_{\text{Ag}}$). There is no phase separation between magnetism and superconductivity; the two coexist microscopically.

Figure 3(b) gives the temperature dependence of σ_{sc} for $\mu_0 H_T = 30$ mT. We obtain $\lambda_{ab}^{-2}(T)$ from Eq. (5), using the temperature dependence of B_{c2} reported in Ref. [25] together with $B_{c2}(0) = 0.5$ T [28] and $T_c = 4.1$ K for our single crystal. Figure 3(c) compares the temperature dependencies of $\sigma_{\text{sc}}(T)/\sigma_{\text{sc}}(0)$ and $\lambda_{ab}^{-2}(T)/\lambda_{ab}^{-2}(0)$. The difference is not large, and both quantities exhibit linear behavior at low temperatures.

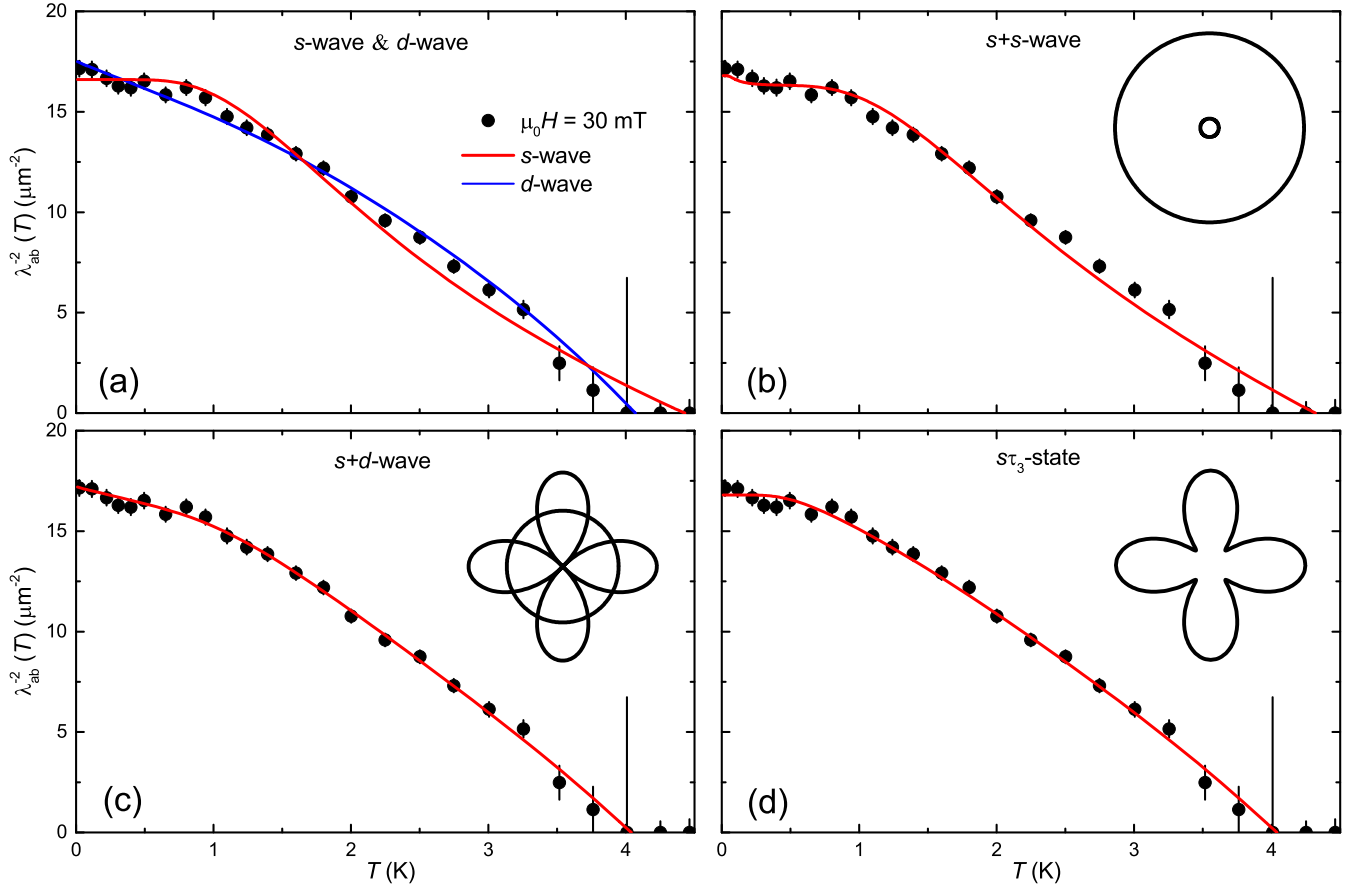


FIG. 4. Temperature dependence of the superfluid density λ_{ab}^{-2} for FeS Sample B with applied field $\mu_0H = 30$ mT. The solid lines are fits for different superconducting gap symmetries. (a) s -wave and d -wave, (b) $s+s$ -wave, (c) $s+d$ -wave, and (d) $s\tau_3$ -state. The corresponding angular dependencies of the superconducting energy gap(s) are shown in insets. See main text for details.

2. Gap symmetry

We fit the relation [17,50,51]

$$\frac{\lambda_{ab}^{-2}(T)}{\lambda_{ab}^{-2}(0)} = 1 + \frac{1}{\pi} \int_0^{2\pi} d\varphi \int_{\Delta(T,\varphi)}^{\infty} dE \frac{\partial f}{\partial E} \frac{E}{\sqrt{E^2 - \Delta^2(T,\varphi)}}, \quad (7)$$

where $f(E)$ is the Fermi function, to the observed temperature dependence of λ_{ab}^{-2} . The gap symmetry enters this expression via the form of $\Delta_s(T,\varphi)$. For the s -wave model $\Delta_s(T,\varphi) = \Delta^s(0)\delta(T/T_c)$, where the temperature dependence $\delta(T/T_c)$ of the relative superconducting gap is estimated using [17,51]

$$\delta(T/T_c) = \tanh \{ 1.82[1.018(T_c/T - 1)]^{0.51} \}. \quad (8)$$

Similarly, $\Delta_d(T,\varphi) = \Delta^d(0)\delta(T/T_c) \cos(2\varphi)$ for the d -wave model. In the recently proposed orbital-selective $s\tau_3$ state for iron selenides [52], the intraband ($d_{x^2-y^2}$) and interband (d_{xy}) nodal pairing terms add in quadrature. As a consequence, the quasiparticle excitation is fully gapped on the Fermi surface. A simplified model of the $s\tau_3$ state gives $\Delta_{s\tau_3}(T,\varphi) = \delta(T/T_c)[(\Delta_1(0) \cos(2\varphi))^2 + (\Delta_2(0) \sin(2\varphi))^2]^{1/2}$ [53]. Finally, for two weakly coupled superconducting bands ($s+s$ or $s+d$), a linear combination

of terms of the form of Eq. (7) can be used [51,54]:

$$\frac{\lambda^{-2}(T)}{\lambda^{-2}(0)} = \omega \frac{\lambda^{-2}(T, \Delta_1(T))}{\lambda^{-2}(0, \Delta_1(0))} + (1 - \omega) \frac{\lambda^{-2}(T, \Delta_2(T))}{\lambda^{-2}(0, \Delta_2(0))}. \quad (9)$$

Fits of s -wave, d -wave, $s+s$ -wave, $s+d$ -wave, and orbital-selective $s\tau_3$ models to our data are shown in Fig. 4. The angular dependencies of the gaps are shown schematically in the insets. It is obvious that the single s -wave and d -wave models do not describe the temperature dependence of λ_{ab}^{-2} accurately. Fit parameters for the three multiband models are shown in Table I. Fits using the $s+s$ -wave model give large values of the reduced chi-square χ_{red}^2 (see also Fig. 4), and the smaller gap (0.02 meV) and its ratio to T_c ($2\Delta_2/k_B T_c = 0.11$) are unreasonably small. This is evidence against $s+s$ pairing symmetry. The discrepancy with previous work [25,26] in this regard reflects differences in $\lambda_{ab}^{-2}(T)$ obtained from polycrystal and single-crystal samples, as discussed below in Sec. III B.

For the $s\tau_3$ model, the larger gaps are four times smaller. This is similar to results in the heavy fermion superconductor CeCu₂Si₂, which is fitted by the same model [53]. The $s\tau_3$ model and $s+d$ -wave describe both sets of data quite well. As noted in Ref. [25], the measured superfluid density λ_{ab}^{-2} is integrated over the entire Fermi surface. Thus it is hard to distinguish slight differences of anisotropy [See Figs. 4(c) and 4(d)]

TABLE I. Parameters from fits of the $s+s$ -wave, $s+d$ -wave, and $s\tau_3$ models to the temperature dependence of $\lambda_{ab}^{-2}(T)$.

Model	$\mu_0 H_T$ (mT)	T_c (K)	$\Delta_1(0)$ (meV)	$2\Delta_1/k_B T_c$	$\Delta_2(0)$ (meV)	$2\Delta_2/k_B T_c$	ω	$\lambda_{ab}^{-2}(0)$ (μm^{-2})	χ_{red}^2
$s+s$ -wave	30	4.32	0.44	2.36	0.02	0.11	0.97	16.8	1.83
$s+d$ -wave	30	4.04(4)	0.43(4)	2.47	0.79(5)	4.54	0.36	17.2	0.53
$s\tau_3$ -state	30	4.04(2)	0.72(2)	4.13	0.16(2)	0.92		16.8	0.74
$s+s$ -wave	75	3.77	0.42	2.56	0.05	0.31	0.92	17.8	2.26
$s+d$ -wave	75	3.63(5)	0.40(5)	2.56	0.68(6)	4.35	0.30	18.0	1.44
$s\tau_3$ -state	75	3.64(4)	0.67(3)	4.27	0.15(3)	0.96		17.5	1.30

over the entire temperature range below T_c . However, the temperature dependence of λ_{ab}^{-2} for these two models is quite different at low temperatures, where the $s+d$ -wave model gives a better description.

Thus our results suggest an $s+d$ -wave pairing state with multiband and nodal superconductivity, and yield in-plane penetration depth $\lambda_{ab}(0) = 241(3)$ nm. Table I shows that the s band and the d band make comparable contributions to the superfluid density, which is consistent with theoretical calculation [29]. Table I also shows that $2\Delta/k_B T_c$ for one gap is less than BCS value of 3.54 and is larger for the other gap. This is consistent with the theoretical constraints [55], and has been observed in many IBS as summarized by Adamski *et al.* [56]. The values of $2\Delta(0)/k_B T_c$ are close for different fields, indicating the self-consistency of the fits.

3. Field dependence

The field dependence of σ_{sc} at low temperatures from our data (denoted by σ_{ab}) and from previous results in polycrystals [25,26] (denoted by σ_{eff}) are compared in Table II.

A maximum near 30 mT is observed in our results and those of Ref. [25], which also shows agreement at higher fields with Eq. (5) (as previously noted [26,49], this relation is not valid at low fields).

The magnitude of σ_{sc} from our single-crystal measurements is remarkably similar to results from polycrystals. As discussed below in Sec. III B, this result is unexpected, and is important for characterizing the superconducting penetration depth in FeS.

III. DISCUSSION

A. Static magnetism

Previous μSR experiments on polycrystalline FeS by Holenstein *et al.* [25] revealed low-moment magnetism below $T_{\text{mag}} \approx 20$ K, whereas no intrinsic static magnetism was reported in other μSR experiments [26] or by neutron scattering

TABLE II. Field dependence of FLL relaxation rate σ_{sc} in FeS at low temperatures.

$\mu_0 H_T$ (mT)	$\sigma_{ab}(\mu\text{S}^{-1})$		$\sigma_{\text{eff}}(\mu\text{S}^{-1})$	
	This work	Ref. [25]	Ref. [25]	Ref. [26]
7.5	0.92	0.96		
15				0.91
30	1.13	0.8–1.03		1.1
75	0.87	0.81		

or transport experiments [31]. Our ZF- μSR experiments on single crystalline FeS confirm the onset of low-moment static magnetism in the ab plane below a lower $T_{\text{mag}} \approx 13$ K, which coexists with superconductivity below T_c . The present results and those of Ref. [25] for the temperature dependencies of Λ_{ZF} and $A(0)$ are more or less consistent, although Ref. [25] does not report an anomaly at 70 K.

We note that the muon depolarization functions are different between our ZF- μSR spectra and those of Ref. [25]: these authors report “root exponential” $\exp[-(\Lambda t)^{1/2}]$ relaxation, whereas we observe simple exponential relaxation. The difference is consistent with our conclusion that the muon local field from the low-moment static magnetism is roughly oriented in the ab -plane, since then it would be more disordered in randomly oriented polycrystalline samples. The root exponential function, which signals a broad distribution of exponential rates [57,58], would then be a better description for ZF- μSR spectra of polycrystalline FeS.

The ZF- μSR study of polycrystalline FeS by Kirschner *et al.* [26] used a sum of two simple exponential functions to describe the muon depolarization. The authors reported a slow relaxation in 85% volume fraction, attributed to intrinsic magnetic moments of the iron in FeS, and a fast relaxation with 15% volume fraction attributed to a magnetic impurity phase. The difference between this result and the root-exponential relaxation reported in Ref. [25] may not be primarily in the data, but instead a consequence of the fact that a fit to data of a relaxation function that is a sum of exponentials often does not determine the coefficients in the sum (or the distribution function in an integral) well; the problem is ill-conditioned [59]. A two-exponential function is difficult to distinguish from a “stretched exponential” $\exp[-(\Lambda t)^\alpha]$ ($\alpha < 1$) unless the two amplitudes are comparable and the rates are very different.

1. Single-crystal/polycrystal sample dependence

Our TF- μSR measurements suggest $s+d$ -wave superconducting pairing symmetry in FeS, with nodal and multiband superconductivity. This differs from the previous μSR results of Refs. [25] and [26] on polycrystals, which reported fully gapped superconductivity based on the absence of a linear $\lambda^{-2}(T)$ at low temperatures. A similar situation arose in early TF- μSR penetration depth measurements on high- T_c cuprates $\text{YBa}_2\text{Cu}_3\text{O}_{7-\delta}$ (YBCO). Experiments on polycrystal materials as well as the first available single crystals indicated an isotropic s -wave order parameter [60,61]. Nodal superconductivity was observed only after experiments on good single-crystalline YBCO revealed a linear-low temperature dependence of penetration depth [62]. The difference has

been attributed to disorder in the earlier samples [63]. In hydrothermal-growth FeS, the impurity phase is a byproduct of the growth process, and has been observed in both polycrystal and single crystal samples. Nevertheless, disorder remains a candidate for the lack of a linear relaxation rate in Fe polycrystals, since single crystals might be less disordered in spite of similar preparation techniques.

Anisotropy in the temperature dependence of the penetration depth is an alternative candidate mechanism for these differences. In polycrystal samples, the corresponding muon relaxation rates σ_{ab} (single crystal, $\mathbf{H}_T \parallel \mathbf{c}$) and σ_{eff} (polycrystal) are related by

$$\sigma_{\text{eff}} = \sigma_{ab}[(3 + \eta)/3(1 + \eta)]^{1/2}, \quad (10)$$

where the anisotropy parameter $\eta = \lambda_c^2/\lambda_{ab}^2 - 1$ [64]. For $\eta \gg 1$,

$$\sigma_{\text{eff}} = \sigma_{ab}/3^{1/2} \quad (\lambda_c \gg \lambda_{ab}), \quad (11)$$

i.e., a long enough λ_c does not affect σ_{eff} .

The in-plane depth λ_{ab} in uniaxial superconductors with strong anisotropy is often estimated from the measured λ_{eff} in polycrystal samples by assuming that $\lambda_{ab} \ll \lambda_c$, so that $\lambda_{\text{eff}} = 3^{1/4}\lambda_{ab}$ ($\lambda \propto \sigma_{\text{sc}}^{-1/2}$) and λ_c plays no role. This assumption was made in Refs. [25] and [26] to obtain the magnitude and temperature dependence of λ_{ab} .

It breaks down, however, if η is not too large (so that λ_c plays a role in λ_{eff}) and if, in addition, the temperature dependence of the penetration depth is not the same for λ_c as for λ_{ab} . This is observed in YBCO, for example [65]. If it is also the case in FeS, and if η is not large, then $\lambda_{\text{eff}} \propto \lambda_{ab}$ is not a good approximation. We test this assumption by comparing single-crystal and polycrystal data from Table II at the same field (30 mT) with Eq. (11). The experimental ratio $\sigma_{\text{eff}}/\sigma_{ab}$ ranges from 0.71 to 1.03, much closer to the isotropic result $\sigma_{\text{eff}}/\sigma_{ab} = 1$ ($\eta = 0$) than the value $3^{-1/2} = 0.577$ for $\eta \gg 1$.

Thus, weakened anisotropy and/or disorder in polycrystals are both candidates for the single-crystal/polycrystal difference. More work will be needed to clarify this situation, including direct measurement of the magnitude and temperature dependence of λ_c in a single crystal.

2. Pairing symmetry

The fits of the models for $\lambda_{ab}^{-2}(T)$ suggest the presence of weakly coupled bands with s -wave (nodeless) and d -wave (nodal) pairing, consistent with other results. ARPES measurements [30] observed two holelike and two electronlike Fermi pockets around the Brillouin zone center and corner,

respectively. Theoretical study suggested that the gap function is nodal/nodeless on the hole/electron Fermi pockets [29]. Scanning tunneling microscopy (STM) experiments [66] showed a V-shaped spectrum, which is well described by both anisotropic s -wave and $s+d$ -wave models. The weight factor and energy gaps of the $s+d$ -wave model fit to the STM spectra are close to our fitting results. Nodal gap behavior is also inferred from low-temperature heat capacity and thermal conductivity measurements [27,28].

It is not surprising that the fits of both $s+d$ -wave and $s\tau_3$ models give comparable goodness of fits. Distinguishing between a very small second gap and no gap (line nodes), or different anisotropy of gap from the μSR data alone is of course very difficult, thus $s+s$ -wave and $s\tau_3$ pairing cannot be conclusively ruled out. The data are, however, fully consistent with the $s+d$ -wave picture that emerges from other studies.

IV. CONCLUSIONS

In summary, we have studied the magnetic and superconducting properties of FeS single crystal samples by μSR . Loss of initial sample asymmetry with decreasing temperature indicates rapid muon relaxation, presumably due to impurities, in 12% of the sample volume, increasing to 15% at the superconducting transition. In the remainder of the sample, low-moment disordered static magnetism is found below $T_{\text{mag}} \approx 13$ K, which coexists microscopically with superconductivity below $T_c = 4.1$ K. A significant T -linear dependence of the in-plane superfluid density λ_{ab}^{-2} is observed at low temperatures, indicating a nodal superconducting gap. The temperature dependencies of the superfluid density are best described by the multiband and nodal superconductivity of the $s+d$ -wave model. The absolute value of the in-plane $T=0$ penetration depth is $\lambda_{ab}^{-2}(0) = 241(3)$ nm.

ACKNOWLEDGMENTS

We are grateful to G. D. Morris, B. Hitti, and D. Arsenau of the TRIUMF CMMS for assistance during the experiments. This research is supported by the National Key Research and Development Program of China (No. 2017YFA0303104 and No. 2016YFA0300503), and the National Natural Science Foundation of China under Grant No. 11474060 and No. 11774061. Work at CSULA was funded by the U.S. NSF DMR/PREM-1523588. Research at CSU Fresno was supported by NSF DMR-1506677. Research at U.C. Riverside was supported by the U.C. Riverside Academic Senate.

[1] Y. Kamihara, T. Watanabe, M. Hirano, and H. Hosono, *J. Am. Chem. Soc.* **130**, 3296 (2008).
 [2] X. Chen, P. Dai, D. Feng, T. Xiang, and F. Zhang, *Nat. Sci. Rev.* **1**, 371 (2014).
 [3] P. Dai, *Rev. Mod. Phys.* **87**, 855 (2015).
 [4] Z. Ren, W. Lu, J. Yang, W. Yi, X. Shen, G. Che, X. Dong, L. Sun, F. Zhou, and Z. Zhao, *Chin. Phys. Lett.* **25**, 2215 (2008).

[5] G. Wu, Y. Xie, H. Chen, M. Zhong, R. Liu, B. Shi, Q. Li, X. Wang, T. Wu, Y. Yan, J. Ying, and X. Chen, *J. Phys.: Condens. Matter* **21**, 142203 (2009).
 [6] A. Subedi, L. Zhang, D. J. Singh, and M. H. Du, *Phys. Rev. B* **78**, 134514 (2008).
 [7] Y. Mizuguchi and Y. Takano, *J. Phys. Soc. Jpn.* **79**, 102001 (2010).

- [8] F. C. Hsu, J. Y. Luo, K. W. Yeh, T. K. Chen, T. W. Huang, P. M. Wu, Y. C. Lee, Y. L. Huang, Y. Y. Chu, D. C. Yan *et al.*, *Proc. Natl. Acad. Sci.* **105**, 14262 (2008).
- [9] S. Medvedev, T. M. McQueen, I. A. Troyan, T. Palasyuk, M. I. Eremets, R. J. Cava, S. Naghavi, F. Casper, V. Ksenofontov, G. Wortmann, and C. Felser, *Nat. Mater.* **8**, 630 (2009).
- [10] Y. Miyata, K. Nakayama, K. Sugawara, T. Sato, and T. Takahashi, *Nat. Mater.* **14**, 775 (2015).
- [11] Q. Wang, Z. Li, W. Zhang, Z. Zhang, J. Zhang, W. Li, H. Ding, Y. Ou, P. Deng, K. Chang, J. Wen, C. Song, K. He, J. Jia, S. Ji, Y. Wang, L. Wang, X. Chen, X. Ma, and Q. Xue, *Chin. Phys. Lett.* **29**, 037402 (2012).
- [12] J. Ge, Z. Liu, C. Liu, C. Gao, D. Qian, Q. Xue, Y. Liu, and J. Jia, *Nat. Mater.* **14**, 285 (2015).
- [13] R. M. Fernandes, A. V. Chubukov, and J. Schmalian, *Nat. Phys.* **10**, 97 (2014).
- [14] T. M. McQueen, A. J. Williams, P. W. Stephens, J. Tao, Y. Zhu, V. Ksenofontov, F. Casper, C. Felser, and R. J. Cava, *Phys. Rev. Lett.* **103**, 057002 (2009).
- [15] S. H. Baek, D. V. Efremov, J. M. Ok, J. S. Kim, J. Van, and B. Büchner, *Nat. Mater.* **14**, 210 (2015).
- [16] A. E. Böhrer, T. Arai, F. Hardy, T. Hattori, T. Iye, T. Wolf, H. V. Löhneysen, K. Ishida, and C. Meingast, *Phys. Rev. Lett.* **114**, 027001 (2015).
- [17] R. Khasanov, K. Conder, E. Pomjakushina, A. Amato, C. Baines, Z. Bukowski, J. Karpinski, S. Katrych, H. H. Klauss, H. Luetkens, A. Shengelaya, and N. D. Zhigadlo, *Phys. Rev. B* **78**, 220510 (2008).
- [18] J. K. Dong, T. Y. Guan, S. Y. Zhou, X. Qiu, L. Ding, C. Zhang, U. Patel, Z. L. Xiao, and S. Y. Li, *Phys. Rev. B* **80**, 024518 (2009).
- [19] C. Song, Y. Wang, P. Cheng, Y. Jiang, W. Li, T. Zhang, Z. Li, K. He, L. Wang, J. Jia, H. Hung, C. Wu, X. Ma, X. Chen, and Q. Xue, *Science* **332**, 1410 (2011).
- [20] X. Lai, H. Zhang, Y. Wang, X. Wang, X. Zhang, J. Lin, and F. Huang, *J. Am. Chem. Soc.* **137**, 10148 (2015).
- [21] J. Zhang, F. Liu, T. Ying, N. Li, Y. Xu, L. He, X. Hong, Y. Yu, M. Wang, J. Shen, W. Yang, and S. Li, *npj Quantum Mat.* **2**, 49 (2017).
- [22] A. Schenck, *Muon Spin Rotation: Principles and Applications in Solid State Physics* (Hilger, Bristol, Boston, 1985).
- [23] J. H. Brewer, in *Encyclopedia of Applied Physics*, Vol. 11, edited by G. L. Trigg, E. S. Vera, and W. Greulich (VCH Publishers, New York, 1994), pp. 23–53.
- [24] A. Yaouanc and P. Dalmas de Réotier, *Muon Spin Rotation, Relaxation, and Resonance: Applications to Condensed Matter* (Oxford University Press, New York, 2011), Vol. 147.
- [25] S. Hohenstein, U. Pachmayr, Z. Guguchia, S. Kamusella, R. Khasanov, A. Amato, C. Baines, H. H. Klauss, E. Morenzoni, D. Johrendt, and H. Luetkens, *Phys. Rev. B* **93**, 140506(R) (2016).
- [26] F. K. K. Kirschner, F. Lang, C. V. Topping, P. J. Baker, F. L. Pratt, S. E. Wright, D. N. Woodruff, S. J. Clarke, and S. J. Blundell, *Phys. Rev. B* **94**, 134509 (2016).
- [27] J. Xing, H. Lin, Y. Li, S. Li, X. Zhu, H. Yang, and H. H. Wen, *Phys. Rev. B* **93**, 104520 (2016).
- [28] T. P. Ying, X. F. Lai, X. C. Hong, Y. Xu, L. P. He, J. Zhang, M. X. Wang, Y. J. Yu, F. Q. Huang, and S. Y. Li, *Phys. Rev. B* **94**, 100504(R) (2016).
- [29] Y. Yang, W.-S. Wang, H.-Y. Lu, Y.-Y. Xiang, and Q.-H. Wang, *Phys. Rev. B* **93**, 104514 (2016).
- [30] J. Miao, X. H. Niu, D. F. Xu, Q. Yao, Q. Y. Chen, T. P. Ying, S. Y. Li, Y. F. Fang, J. C. Zhang, S. Ideta, K. Tanaka, B. P. Xie, D. L. Feng, and F. Chen, *Phys. Rev. B* **95**, 205127 (2017).
- [31] H. Man, J. Guo, R. Zhang, R. Schönemann, Z. Yin, M. Fu, M. B. Stone, Q. Huang, Y. Song, W. Wang *et al.*, *NPJ Quantum Mat.* **2**, 14 (2017).
- [32] C. Tresca, G. Giovannetti, M. Capone, and G. Profeta, *Phys. Rev. B* **95**, 205117 (2017).
- [33] C. K. H. Borg, X. Zhou, C. Eckberg, D. J. Campbell, S. R. Saha, J. Paglione, and E. E. Rodriguez, *Phys. Rev. B* **93**, 094522 (2016).
- [34] H. Lin, Y. Li, Q. Deng, J. Xing, J. Liu, X. Zhu, H. Yang, and H. H. Wen, *Phys. Rev. B* **93**, 144505 (2016).
- [35] J. H. Brewer, *Hyperfine Interact.* **230**, 35 (2015).
- [36] Silver is used because its weak nuclear magnetism results in negligible muon relaxation.
- [37] R. Kubo and T. Toyabe, in *Magnetic Resonance and Relaxation*, edited by R. Blinc (North-Holland, Amsterdam, 1967) pp. 810–823.
- [38] R. S. Hayano, Y. J. Uemura, J. Imazato, N. Nishida, T. Yamazaki, and R. Kubo, *Phys. Rev. B* **20**, 850 (1979).
- [39] Y. J. Uemura, T. Yamazaki, D. R. Harshman, M. Senba, and E. J. Ansaldo, *Phys. Rev. B* **31**, 546 (1985).
- [40] See, e.g., Ref. [24], Sec. 6.2.2.
- [41] P. Dalmas de Réotier and A. Yaouanc, *J. Phys.: Condens. Matter* **9**, 9113 (1997).
- [42] U. Pachmayr, N. Fehn, and D. Johrendt, *Chem. Commun.* **52**, 194 (2016).
- [43] M. Bendele, A. Ichsanow, Y. Pashkevich, L. Keller, T. Strässle, A. Gusev, E. Pomjakushina, K. Conder, R. Khasanov, and H. Keller, *Phys. Rev. B* **85**, 064517 (2012).
- [44] A. J. Drew, C. Niedermayer, P. J. Baker, F. L. Pratt, S. J. Blundell, T. Lancaster, R. H. Liu, G. Wu, X. H. Chen, I. Watanabe, V. K. Malik, A. Dubroka, M. Rossle, K. W. Kim, C. Baines, and C. Bernhard, *Nat. Mater.* **8**, 310 (2009).
- [45] M. Bendele, A. Amato, K. Conder, M. Elender, H. Keller, H. H. Klauss, H. Luetkens, E. Pomjakushina, A. Raselli, and R. Khasanov, *Phys. Rev. Lett.* **104**, 087003 (2010).
- [46] Z. Shermadini, A. Krzton-Maziopa, M. Bendele, R. Khasanov, H. Luetkens, K. Conder, E. Pomjakushina, S. Weyeneth, V. Pomjakushin, O. Bossen, and A. Amato, *Phys. Rev. Lett.* **106**, 117602 (2011).
- [47] E. H. Brandt, *Phys. Rev. B* **37**, 2349 (1988).
- [48] J. E. Sonier, J. H. Brewer, and R. F. Kiefl, *Rev. Mod. Phys.* **72**, 769 (2000).
- [49] E. H. Brandt, *Phys. Rev. B* **68**, 054506 (2003).
- [50] M. Tinkham, *Introduction to Superconductivity*, 2nd ed. (McGraw-Hill Book Co., New York, 1996).
- [51] R. Khasanov, A. Shengelaya, A. Maisuradze, F. L. Mattina, A. Bussmann-Holder, H. Keller, and K. A. Müller, *Phys. Rev. Lett.* **98**, 057007 (2007).
- [52] E. M. Nica, R. Yu, and Q. Si, *NPJ Quantum Mat.* **2**, 24 (2017).
- [53] G. M. Pang, M. Smidman, J. L. Zhang, L. Jiao, Z. F. Weng, E. M. Nica, Y. Chen, W. B. Jiang, Y. J. Zhang, H. S. Jeevan, H. Lee, P. Gegenwart, F. Steglich, Q. Si, and H. Q. Yuan, *PNAS* **115**, 5343 (2018).
- [54] M.-S. Kim, J. A. Skinta, T. R. Lemberger, W. N. Kang, H.-J. Kim, E.-M. Choi, and S.-I. Lee, *Phys. Rev. B* **66**, 064511 (2002).
- [55] T. Saito, S. Onari, and H. Kontani, *Phys. Rev. B* **88**, 045115 (2013).

- [56] A. Adamski, C. Krellner, and M. Abdel-Hafiez, *Phys. Rev. B* **96**, 100503 (2017).
- [57] D. C. Johnston, *Phys. Rev. B* **74**, 184430 (2006).
- [58] I.e., the local field distribution is broader than Lorentzian.
- [59] W. H. Press, S. A. Teukolsky, W. T. Vetterling, and B. P. Flannery, *Numerical Recipes in C*, 2nd ed. (Cambridge University Press, New York, 1992), Chap. 18.
- [60] D. R. Harshman, L. F. Schneemeyer, J. V. Waszczak, G. Aeppli, R. J. Cava, B. Batlogg, L. W. Rupp, E. J. Ansaldo, and D. L. Williams, *Phys. Rev. B* **39**, 851 (1989).
- [61] B. Pümpin, H. Keller, W. Kündig, W. Odermatt, I. M. Savić, J. W. Schneider, H. Simmler, P. Zimmermann, E. Kaldis, S. Rusiecki, Y. Maeno, and C. Rossel, *Phys. Rev. B* **42**, 8019 (1990).
- [62] W. N. Hardy, D. A. Bonn, D. C. Morgan, R. Liang, and K. Zhang, *Phys. Rev. Lett.* **70**, 3999 (1993).
- [63] P. J. Hirschfeld and N. Goldenfeld, *Phys. Rev. B* **48**, 4219 (1993).
- [64] V. I. Fesenko, V. N. Gorbunov, and V. P. Smilga, *Physica C (Amsterdam)* **176**, 551 (1991).
- [65] R. Khasanov, S. Strässle, D. Di Castro, T. Masui, S. Miyasaka, S. Tajima, A. Bussmann-Holder, and H. Keller, *Phys. Rev. Lett.* **99**, 237601 (2007).
- [66] X. Yang, Z. Du, G. Du, Q. Gu, H. Lin, D. Fang, H. Yang, X. Zhu, and H.-H. Wen, *Phys. Rev. B* **94**, 024521 (2016).